Developing the Processing Maps Using the Hyperbolic Sine Constitutive Equation

AMIR MOMENI, KAMRAN DEHGHANI, GOLAM REZA EBRAHIMI, and SHAHAB KAZEMI

Hot compression tests were performed on a duplex stainless steel at temperatures ranging from 1223 K to 1473 K (950 °C to 1200 °C) and strain rates from 0.001 to 100 s^{-1}. The constitutive analysis of flow stress was carried out using the hyperbolic sine function, and the material constants were determined at two typical strains of 0.3 and 0.7. The power dissipation map, instability map, and processing map for the material were developed for strains of 0.3 and 0.7. The developed processing maps were based on the hyperbolic sine as well as the conventional power-law constitutive equations. The efficiency of power dissipation (η) varied from 12 to 60 pct over the studied temperature and strain rate. The highest value of η was obtained at strain rates below 0.01 s^{-1}, whereas the lowest value of η was observed at the intermediate strain rates. The instability region in sin h-based processing map was only observed in the range of 1423 K to 1473 K (1150 °C to 1200 °C) and at a strain rate of 100 s^{-1}, while the conventional processing map did not predict any instability region. Optical microscopy observations were more consistent with the results of the sin h-based processing map and indicated that the instability regime at high temperatures and high strain rates was due to the development of adiabatic shear bands.

DOI: 10.1007/s11661-013-1841-5

I. INTRODUCTION

THE prediction of flow stress and load needed for the deformation of an alloy is an important step for the design of an industrial hot-working operation. The flow stress is closely related to the both intrinsic and extrinsic workabilities of the material being deformed. The intrinsic workability is governed by the mechanisms of microstructural changes at a given deformation condition. However, the processing variables, *i.e.*, strain, strain rate, and temperature actually control the microstructural evolutions and thereby the intrinsic and extrinsic workabilities of a material. Different constitutive equations have been used to interconnect the mentioned workability factors and derive an applicable formula for measuring the flow stress as a function of processing variables.[1–3] Even though the constitutive equations are widely used to estimate the deformation loads, the behavior of the material in terms of stable or unstable flow should be also analyzed. One of the well-developed practical methods to avoid the occurrence of an unstable flow and premature fracture is plotting a processing map. The approach of processing map, originally proposed by Raj.[4] is defined as a representation of microstructural changes and restoration mechanisms of a given material. However, some questions still arise about the reliability of this method.[5] A processing map illustrates a superimposition of power dissipation map (PDM) and instability regions which are depicted on the basis of dynamic materials model (DMM).[6] DMM is a continuum model in which an instability criterion based on the principles of irreversible thermodynamic, as applied to large plastic flow, is utilized to mark flow instability regimes.[7] The power dissipation and the instability maps are plotted in terms of deformation temperature and logarithm of strain rate to correlate different regions with the processing variables. The principles of this approach and its applications to the hot deformation of a wide range of materials were described by Prasad and other researchers.[8–11]

In the DMM model, the constitutive equation used to relate the flow stress to strain rate and temperature is of power-law type, as follows:

$$\sigma = K\dot{\varepsilon}^m \qquad [1]$$

where K is a temperature-dependent constant and m stands for the strain rate sensitivity parameter. This equation gives a good measurement of the behavior of the workpiece when it consumes the energy as a visco-plastic material. While in case of many metallic materials, Eq. [1] is actually applicable at high temperatures and low strain rates, such as creep, not at hot working conditions. It has been well-documented that many

AMIR MOMENI, Assistant Professor, is with the Department of Materials Science and Engineering, Hamedan University of Technology, Hamedan, Iran. Contact e-mail: ammomeni@aut.ac.ir KAMRAN DEHGHANI, Associate Professor, is with the Department of Mining and Metallurgy, Amirkabir University of Technology, Tehran, Iran. GOLAM REZA EBRAHIMI, Associate Professor, is with the Department of Materials and Polymer Engineering, Hakim Sabzevari University, Sabzevar, Iran. SHAHAB KAZEMI, Assistant Professor, is with the D. M. S. E., Bu Ali Sina University, Hamedan, Iran.

Manuscript submitted October 14, 2012.
Article published online June 28, 2013

alloys subjected to hot deformation obey a hyperbolic sine constitutive equation,[12–16] that was originally proposed by Garofalo[17] as follow:

$$Z = \dot{\varepsilon} \exp\left(\frac{Q}{RT}\right) = A\,[\sin\, h(\alpha \cdot \sigma)]^n. \qquad [2]$$

Here, Z denotes the Zener–Hollomon parameter; Q is the activation energy; and A, α, and n are the material constants. This widely used equation is indeed reduced to power-law [Eq. 1] and exponential equations, respectively, at low and high stress levels.[18] Although this equation is proved to give a better description of flow stress than the exponential or power-law equations, it has not been used as a basic constitutive equation to develop the processing maps. Narayana Murty *et al.*[19–22] in a set of publications on developing processing maps, tried to simplify the corresponding calculations and used other methods instead of the power-law equation. But they didn't report a considerable difference between the processing maps developed by different methods.

The present investigation has been therefore devoted to study the development of processing maps using the hyperbolic sine constitutive equation. In this research, a very applicable duplex stainless steel designated as 2205 has been analyzed. This alloy is widely used in different industries and its hot working behavior is challenging due to the duplex nature of its microstructure.

II. EXPERIMENTAL PROCEDURES

The material used in this study is 2205 duplex stainless steel with the composition: 0.025 pct C, 22.80 pct Cr, 5.20 pct Ni, 2.60 pct Mo, 0.30 pct Si, 1.50 pct Mn, 0.001 pct S, 0.025 pct P, 0.088 pct V, 0.23 pct Cu, 0.03 pct W, 0.068 pct Co, 0.028 pct Al, and the rest of Fe (all in wt pct). The starting microstructure of the studied material consisting of about 54 pct ferrite and 45 pct austenite is illustrated in Figure 1. The cylindrical specimens, 10-mm diameter and 15-mm height, were prepared from the as-received hot-rolled plate with the longitudinal axis parallel to the rolling direction. Before testing, all specimens were reheated to 1473 K (1200 °C), soaked for 5 minutes, and then subjected to hot compression tests at the temperatures ranging from 1223 K to 1473 K (950 °C to 1200 °C) and strain rates from 0.001 to 100 s^{-1} using a Gleeble 3800 thermomechanical simulator. Graphite powder was applied on both surfaces of specimens to reduce friction coefficient between the specimen ends and the anvils. To preserve microstructures developed during hot deformation, samples were quenched within three seconds after hot deformation. Hotdeformed specimens were cut along the longitudinal axis and electrochemically polished. Following this, electrolytical etching in a 60 pct solution of HNO_3 was adopted to reveal microstructures. Finally, an optical microscopy was used to characterize the microstructures of the deformed samples.

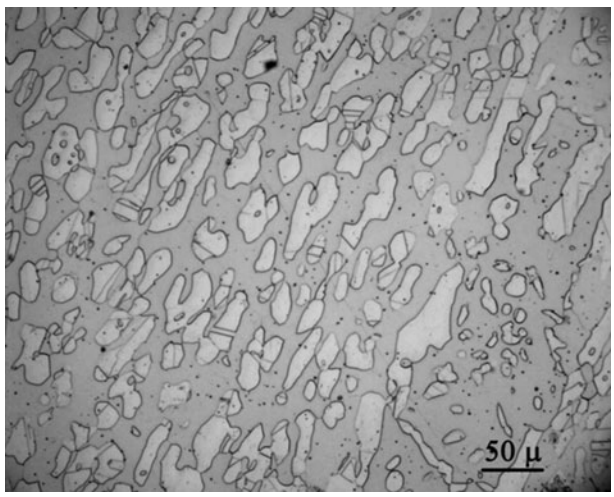

Fig. 1—Starting microstructure of the 2205 duplex stainless steel used in this investigation.

III. RESULTS AND DISCUSSION

A. *Constitutive Analysis*

Figure 2 demonstrates the flow curves obtained from hot compression testing at different deformation conditions. The flow curves approve the generally accepted rules that the flow curve increases as temperatures decreases or strain rate rises. Moreover, the flow curves are different with the flow curves that are typically observed when either dynamic recrystallization (DRX) or dynamic recovery (DRV) are controlling. The typical flow curves of DRX are usually characterized by a peak following which flow softening attains a steady-state behavior. In case of DRV, flow curve indicates a long plateau after work hardening stage. The obtained flow curves indicate that most of them have shapes in between the typical DRX and DRV curves.

The special form of the curves can be directly related to the duplex structure of 2205 steel and has been analyzed by Momeni and Dehghani.[23] Because austenite is prone to DRX and ferrite is instead softened by DRV, the flow curves of 2205 inherit some aspects from the two different kinds of DRV and DRX flow curves. At a high temperature like 1373 K (1100 °C) and especially at low strain rates where ferrite is dominant, flow curves are analogous to the DRV curves with a long plateau of steady-state flow. On the contrary, at low temperature of 1223 K (950 °C) and high strain rates, the harder phase that is austenite starts to work harden, and the flow curve is characterized by the typical form of DRX flow curves.

In general, the hyperbolic sine function [Eq. 2] is the most applicable equation that connects the flow stress at a given strain value to strain rate and temperature over a wide range of applied deformation conditions. In order to determine the material constants, the logarithmic form of Eq. [2] that is given below is more useful:

$$\ln \dot{\varepsilon} = \left(\ln A - \frac{Q}{RT}\right) + n \ln \sin h(\alpha \cdot \sigma). \qquad [3]$$

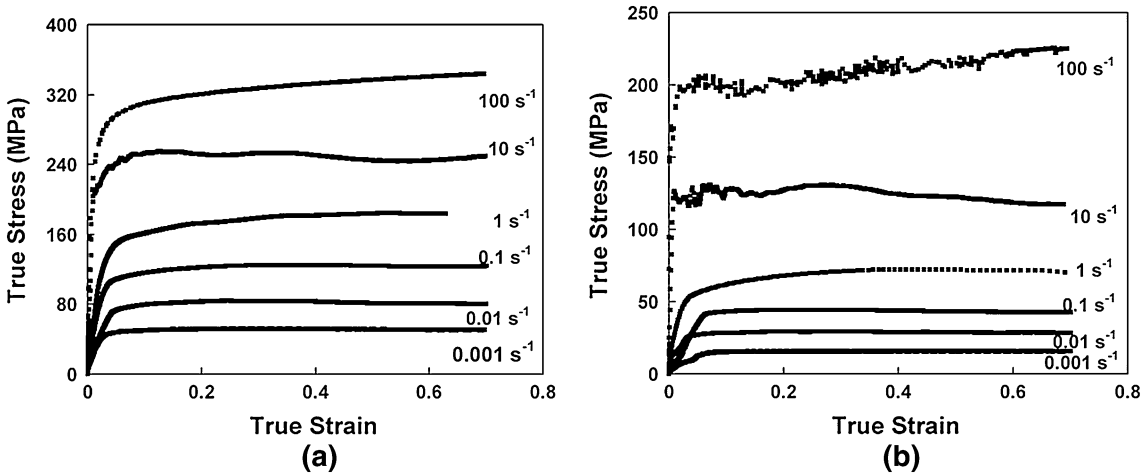

Fig. 2—True stress–true strain curves obtained at (*a*) 1223 K (950 °C) and (*b*) 1373 K (1100 °C).

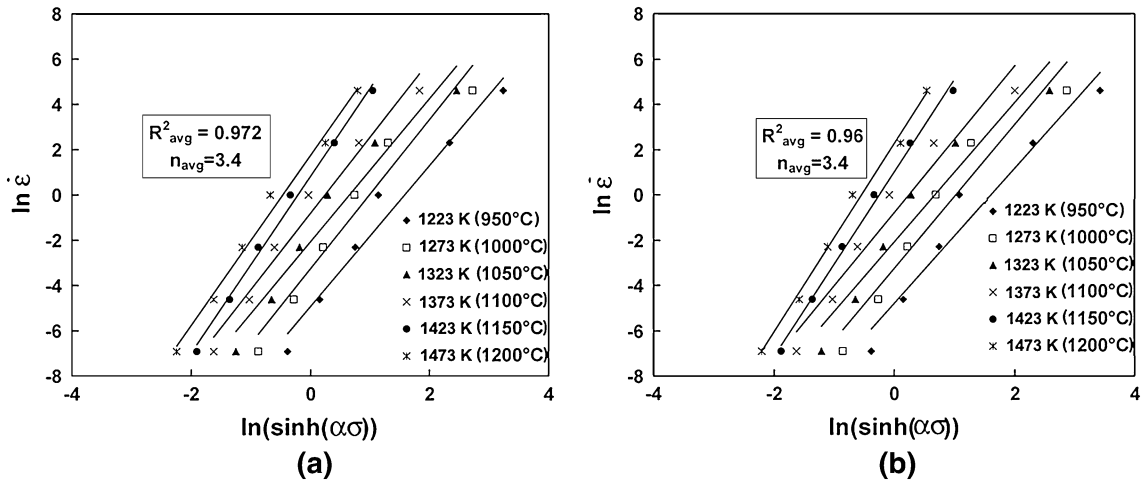

Fig. 3—Variations of flow stress with strain rate in the frame of the hyperbolic sine functions and at strains of (*a*) 0.3 and (*b*) 0.7.

The value of n is simply determined as the partial differentiation of strain rate with respect to the flow stress at a constant temperature, given by

$$n = \frac{\partial \ln \dot{\varepsilon}}{\partial \ln \sin h(\alpha \cdot \sigma)}. \quad [4]$$

In a similar way, Q is evaluated from the first derivative of stress respecting the inverse of temperature, as follows:

$$Q = nR \frac{\partial \ln \sin h(\alpha \cdot \sigma)}{\partial (1/T)}. \quad [5]$$

Using this procedure, the obtained experimental data were processed at two strain values of 0.3 and 0.7 to show the behaviors of the material at both low and high strain levels. Figure 3 indicates the plot of strain rate *vs* flow stress according to Eq. [4].

The high value of correlation factor reflects that Eq. [2] suitably fits the experimental data. The average value of n at both strain levels is nearly the same as 3.4. However, as the authors declared in the previous publications, n value actually depends on the deformation temperature because it is sensitive to the dominant phase in the microstructure.[23] Through the mentioned procedure, α was adjusted as 0.012 so that it brings the curves to the most linear and parallel condition.

The plots of flow stress against $1/T$, shown in Figure 4, are depicted according to Eq. [5] and used to determine the value of the apparent activation energy. By using the average slope of the curves (S_{avg}) that is equal to $\partial \ln \sin h(\alpha\sigma)/\partial(1/T)$, the values of Q were calculated as 405 and 420 kJ mol^{-1} for strains of 0.3 and 0.7, respectively. Figure 5 indicates how the experimental data of flow stress at two strains of 0.3 and 0.7 fit to the frame of the hyperbolic sine function.

In order to make a comparison between the conventional processing maps based on Eq. [1] and the sin h-based processing map, the average values of the strain rate sensitivity parameter (m) are determined and shown in Figure 6 for two strains of 0.3 and 0.7. It should be noted that m is a key parameter in developing the

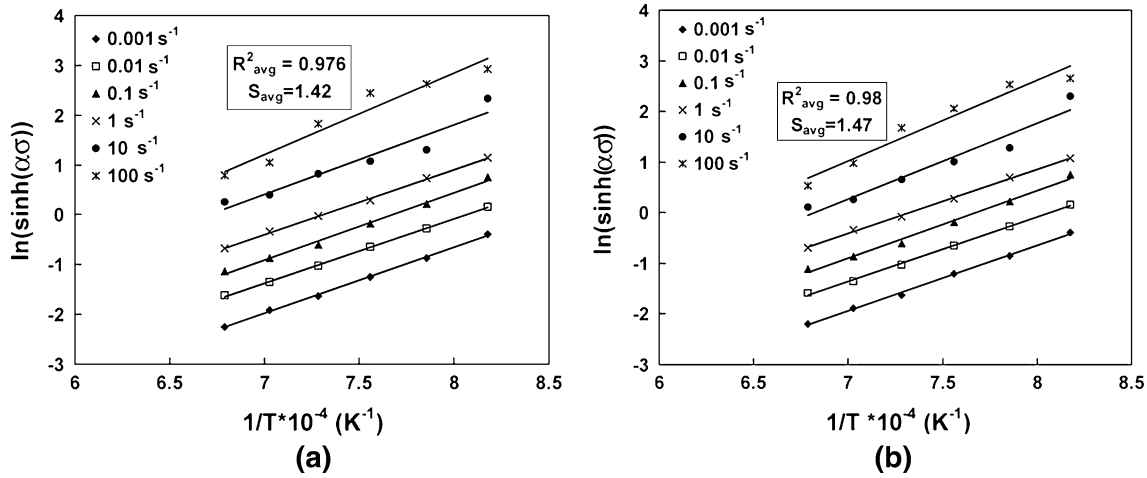

Fig. 4—Plots of the hyperbolic sine of flow stress versus the inverse of temperature ar different strain rates and strains of (*a*) 0.3 and (*b*) 0.7. S_{avg} indicates the average slope of the curves.

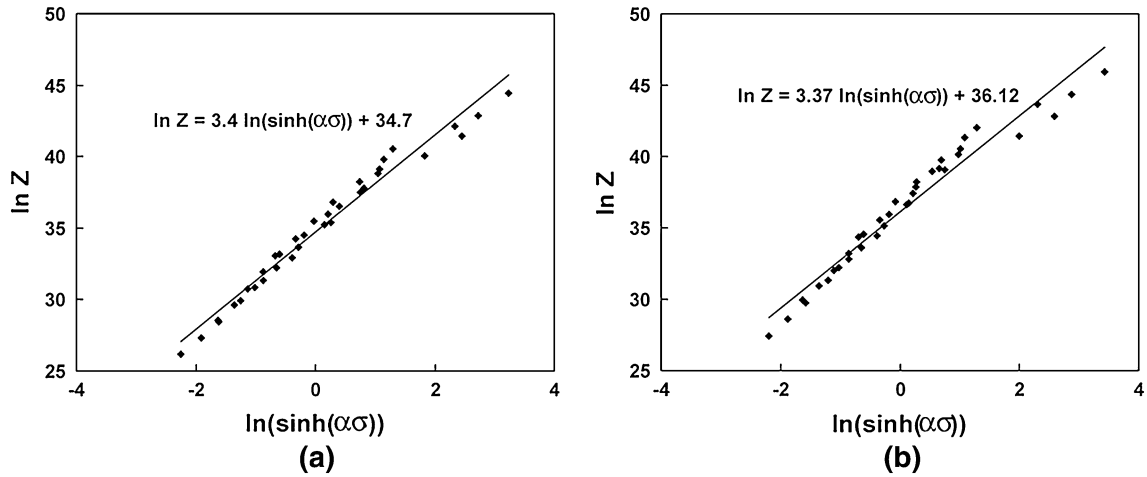

Fig. 5—Variation of Zener–Hollomon parameter with flow stress according to the hyperbolic sine functions at two strains of (*a*) 0.3 and (*b*) 0.7.

processing maps, since it determines the partitioning of income energy between the heat generation and microstructural evolution parts. This parameter is simply determined at different temperatures using the logarithmic form of Eq. [1].

B. *Developing Processing Maps*

A processing map is plotted based on the PDM which represents the response of a material to the applied strain rate at a constant temperature. The response of a material emerging as the effective stress is characterized by constitutive equations. Although the power-law constitutive equation [Eq. 1] is often used in developing the processing maps, as mentioned above, the hyperbolic sine equation, however, is more convincing both at low and high stress levels. Prasad[9] stated that the total dissipated power absorbed by the workpiece (P) is actually the sum of two complementary terms of G and J. The former term contains the power dissipated by the plastic work, and the latter refers to the energy or work dissipated by the dynamic microstructural changes. The total dissipated power can therefore be written as follows:

$$P = J + \mathrm{G} = \sigma\dot{\varepsilon} = \int_0^{\sigma} \dot{\varepsilon}\mathrm{d}\sigma + \int_0^{\dot{\varepsilon}} \sigma\mathrm{d}\dot{\varepsilon}. \qquad [6]$$

It is important to compare the J co-content with a reference or an ideal state having the highest rate of energy consumption through the microstructural changes. It should be noted that the most happening microstructural changes are DRX and DRV which hinder the flow instability to take place. However, some other phenomena such as wedge cracks are not preferable. Therefore, it is better to be careful about this statement that the higher the J co-content, the better the workability of material. The J co-content can be therefore defined as follows:

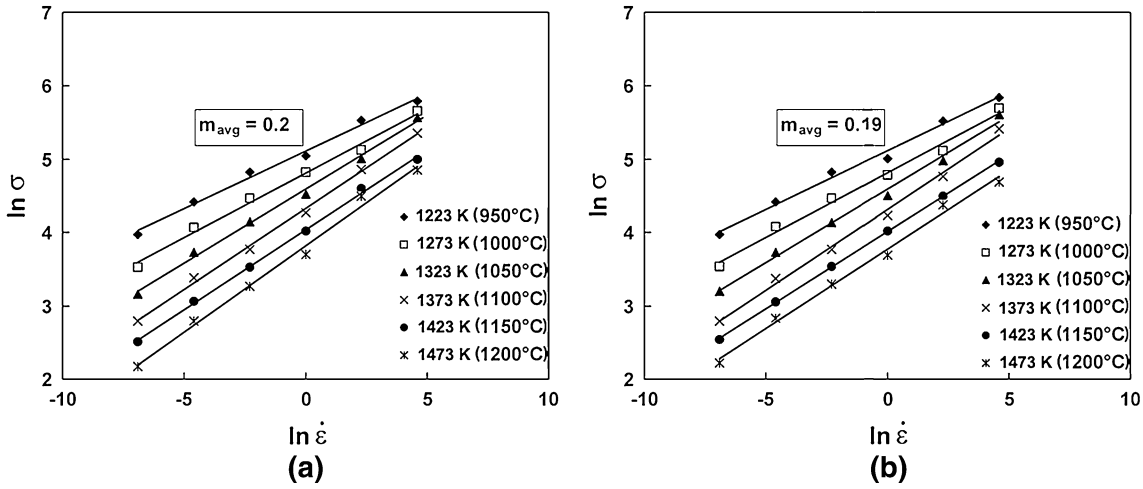

Fig. 6—Variations of flow stress with strain rate in a logarithmic scale according to the power-law constitutive equation at strains of (*a*) 0.3 and (*b*) 0.7.

$$J = \sigma\dot{\varepsilon} - G = \sigma\dot{\varepsilon} - \int_0^{\dot{\varepsilon}} \sigma \mathrm{d}\dot{\varepsilon}. \qquad [7]$$

Therefore, the J co-content can be determined if an appropriate constitutive description of σ is presented for the studied material. As mentioned in the previous section, the hyperbolic sine function suitably describes the connection between flow stress, strain rate, and temperature. The flow stress can be determined from Eq. [2] as follows:

$$\sigma = \frac{1}{\alpha}\sin\mathrm{h}^{-1}\left[\dot{\varepsilon}\left(\frac{1}{A}\exp\left(\frac{Q}{RT}\right)\right)\right]^{1/n}. \qquad [8]$$

Figure 7 indicates that Eq. [8] gives a reasonable measurement of flow stress at different strain rates and deformation temperatures.

The accuracy of this model is satisfactory enough to imply the combination of this constitutive equation of flow stress with Eq. [7]. Hence, after some algebraic operations, the G content can be written as follows:

$$G = \int_0^{\dot{\varepsilon}} \sigma \mathrm{d}\dot{\varepsilon} = \int_0^{\dot{\varepsilon}} \frac{1}{\alpha}\sin\mathrm{h}^{-1}\left[\dot{\varepsilon}\left(\frac{1}{A}\exp\left(\frac{Q}{RT}\right)\right)\right]^{1/n} d\dot{\varepsilon}$$
$$= \frac{1}{\alpha}\left[\dot{\varepsilon}\left(\sin\mathrm{h}^{-1}\left\{\left(\frac{1}{A}\exp\left(\frac{Q}{RT}\right)\dot{\varepsilon}\right)^{1/n} - \frac{\left[\left(\frac{1}{A}\exp\left(\frac{Q}{RT}\right)\dot{\varepsilon}\right)^{1/n} f(\dot{\varepsilon})\right]}{1+n}\right\}\right)\right] \qquad [9]$$

where, $f(\dot{\varepsilon})$ is a hypergeometric function, given by

$$f(\dot{\varepsilon}) = \text{Hypergeometric 2F1}\left[1/2,\ (1+n)/2,\ (3+n)/2,\ \left(-\left[\frac{1}{A}\exp\left(\frac{Q}{RT}\right)\dot{\varepsilon}\right]^{2/n}\right)\right] \qquad [10]$$

The value of the hypergeometric function of Eq. [10] is calculated using the values of n, Q, and A determined in the previous section. Table I summarizes the values of the hypergeometric function at different temperature and strain rates.

According to DMM, the J content of a material can be evaluated with respect to that of an ideal linear dissipater which is as $G = J = (1/2)\sigma\varepsilon$. Using this definition, the dimensionless efficiency of power dissipation, η, can be written as follows:

$$\eta = \frac{J}{J_{\max}} = \frac{J}{\sigma\dot{\varepsilon}/2}. \qquad [11]$$

Therefore, to construct the PDM of a material based on the hyperbolic sine equation a combination of Eqs. [7], [9], and [11] are to be used to determine η at different deformation conditions. In conventional processing maps which are based on Eq. [1], η is simply written as a function of m, given by

$$\eta = \frac{J}{J_{\max}} = \frac{2m}{m+1}. \qquad [12]$$

It should be noted again that a high value of η (*e.g.*, >60 pct) is not always preferable because some instability mechanisms such as wedge cracks may contribute in such a high efficiency of power consumption.[24]

Figure 8 demonstrates the values of η calculated based on the sin h equation at different deformation conditions in the frame of strain rate and temperature. In this figure, the counter numbers represent the efficiency of power dissipation. The calculated η values range between 12 and 60 suggesting fairly good workability of the studied material. Higher η values are observed at low strain rates (actually below 1 s^{-1}) where DRV in ferrite seems to be responsible for the extension, unraveling the strain energy.

Although, more than likely, the regions with higher η values can be regarded as the safer regions for hot working, DMM is capable of introducing the regions of low stability. Ziegler[7] considered the stability of a given material during hot deformation *via* DMM approach

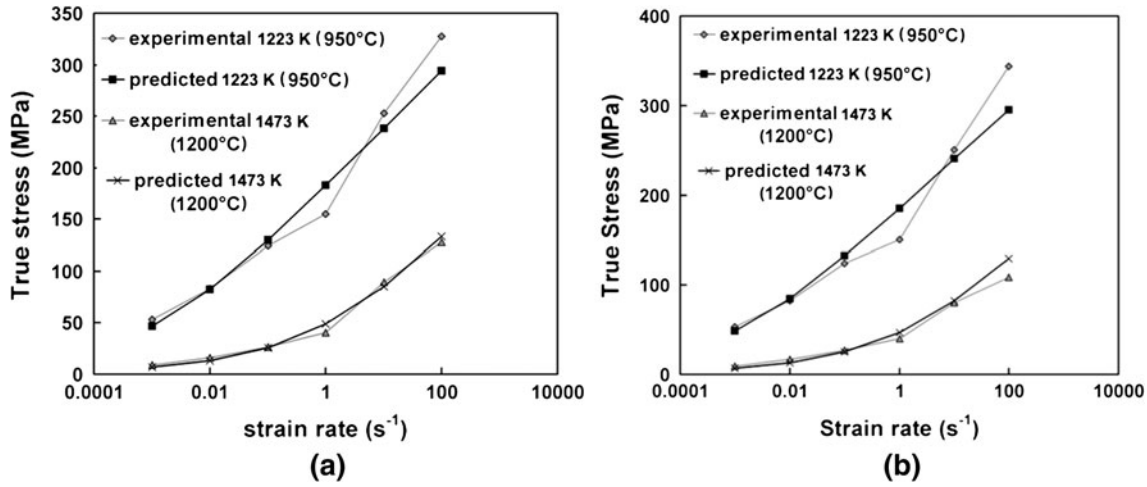

Fig. 7—Comparison of experimental flow stress and predicted values using the developed hyperbolic sine constitutive equations at different strain rates and strains of (*a*) 0.3 and (*b*) 0.7.

Table I. Values of the Hypergeometric Function in Eq. [10] at Different Deformation Temperatures and Strain Rates

	0.001 s^{-1}	0.01 s^{-1}	0.01 s^{-1}	1 s^{-1}	10 s^{-1}	100 s^{-1}
1223 K (950 °C)	0.899	0.727	0.481	0.272	0.143	0.73
1273 K (1000 °C)	0.955	0.856	0.651	0.406	0.223	0.116
1323 K (1050 °C)	0.98	0.93	0.791	0.558	0.328	0.175
1373 K (1100 °C)	0.99	0.966	0.885	0.701	0.455	0.254
1423 K (1150 °C)	0.995	0.983	0.938	0.815	0.588	0.352
1473 K (1200 °C)	0.998	0.992	0.968	0.892	0712	0.465

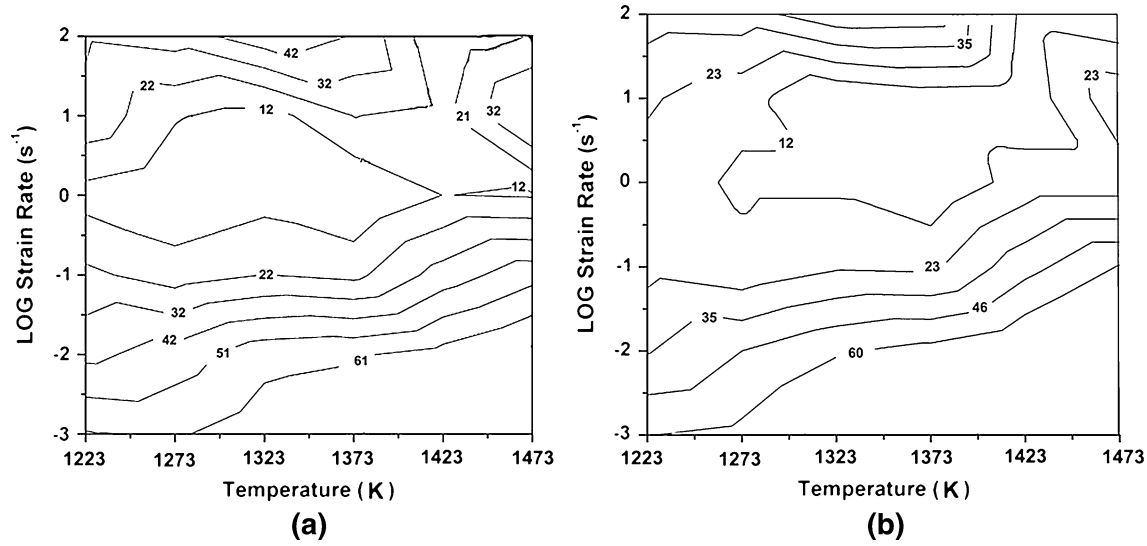

Fig. 8—Sin h-based power dissipation map developed at strains of (*a*) 0.3 and (*b*) 0.7. Each counter number represents the efficiency of power dissipation in pct.

and proposed that stable flow is ensured if the following inequality is satisfied:

$$\frac{\mathrm{d}J}{\mathrm{d}\dot{\varepsilon}} > \frac{J}{\dot{\varepsilon}}. \qquad [13]$$

Therefore, the stability condition can be summarized as the following inequality:

$$\frac{\mathrm{d}\ln J}{\mathrm{d}\ln \dot{\varepsilon}} > 1. \qquad [14]$$

In conventional processing maps based on Eq. [1], Eqs. [1], [7], and [14] are combined to define a stability parameter (ξ) that simplifies the stability condition as follows:

Table II. Values of $d \ln J/d \ln \dot{\varepsilon}$ at Two Typical Strains of 0.3 and 0.7 Calculated Using the Numerical Approach of Eq. [16]

Temperature	Strain Rate (s^{-1})	$(d \ln J/d \ln \dot{\varepsilon})$ at $\varepsilon = 0.3$	$(d \ln J/d \ln \dot{\varepsilon})$ at $\varepsilon = 0.7$
1223 K (950 °C)	0.001	1	1
	0.01	20.8	20.3
	0.1	16.8	21.2
	1	25.3	25.6
	10	31.1	28.5
	100	1 2	1.3
1273 K (1000 °C)	0.001	1.1	1.1
	0.01	19.8	19.1
	0.1	11.3	17.6
	1	23	24.5
	10	37.3	31.8
	100	1.7	1.7
1323 K (1100 °C)	0.001	1.2	1.1
	0.01	20.7	20
	0.1	15.4	16.6
	1	19.9	8.7
	10	34.6	34.3
	100	2.1	3.2
1373 K (1050 °C)	0.001	1.2	1.2
	0.01	19.6	19.9
	0.1	10.1	11.2
	1	27.1	19.9
	10	39.7	39.9
	100	1.5	2.2
1423 K (1150 °C)	0.001	1.1	1.1
	0.01	22.1	22.4
	0.1	17.9	19.3
	1	23.2	15.7
	10	25.9	22.2
	100	1	1.4
1473 K (1200 °C)	0.001	1.2	1.2
	0.01	23.8	24.1
	0.1	16.8	17.8
	1	26.5	23.5
	10	29.7	15.4
	100	0.9	−0.1

$$\xi(\dot{\varepsilon}) = \frac{\partial \ln\left(\frac{m}{m+1}\right)}{\partial \ln \dot{\varepsilon}} + m > 0. \quad [15]$$

In order to use Eq. [2] as the constitutive equation, the stability condition should be considered in its original form [Eq. 14]. However, it is possible to present a numerical approach to solve the inequality of Eq. [14] using the definition of first order derivation as follows:

$$\frac{\ln J(\dot{\varepsilon}_1) - \ln J(\dot{\varepsilon}_2)}{\ln \dot{\varepsilon}_1 - \ln \dot{\varepsilon}_2}\Big|_{\varepsilon,T} > 1. \quad [16]$$

Table II summarizes the values of $d \ln J/d \ln \dot{\varepsilon}$ as calculated from Eq. [16] at different deformation regimes. It is observed that except at 1473 K (1200 °C) and 100 s^{-1}, at other deformation conditions, the condition of stability according to Eq. [14] is met. The complete processing maps exhibited in Figure 9 have been plotted by superimposing Figure 8 and the instability predictions according to Eq. [16].

The hot deformation regimes out of the dark regions on the processing map of the material indicated in Figure 9, should result in a stable flow due to the occurrence of different dynamic restoration processes, *i.e.,* DRX in austenite and DRV in ferrite. It is well known that the dynamic softening mechanisms release the stored deformation energy by dislocation annihilation or by the formation of new dislocation-free grains. The structural modifications caused by dynamic softening mechanisms degrade the strain accumulation and therefore prevent the formation of voids, triple-junction (wedge) cracking, or shear bands.

In a parallel way, the processing map of the material was also developed, as shown in Figure 10, using the conventional method described by Eqs. [12] and [15]. As observed, the conventional processing map predicts the stable flows at all the studied deformation conditions. This indicates that the conventional processing maps have more optimistic predictions regarding instability compared with the processing maps of Figure 9. Moreover, the contours of η in the conventional processing map are more irregular than in Figure 9. Meanwhile, it should be taken into account that, at low strain rates, DRV in the ferritic matrix is expected to proceed expeditiously and therefore cause a higher η value that is more consistent with the sin h-based processing maps. It

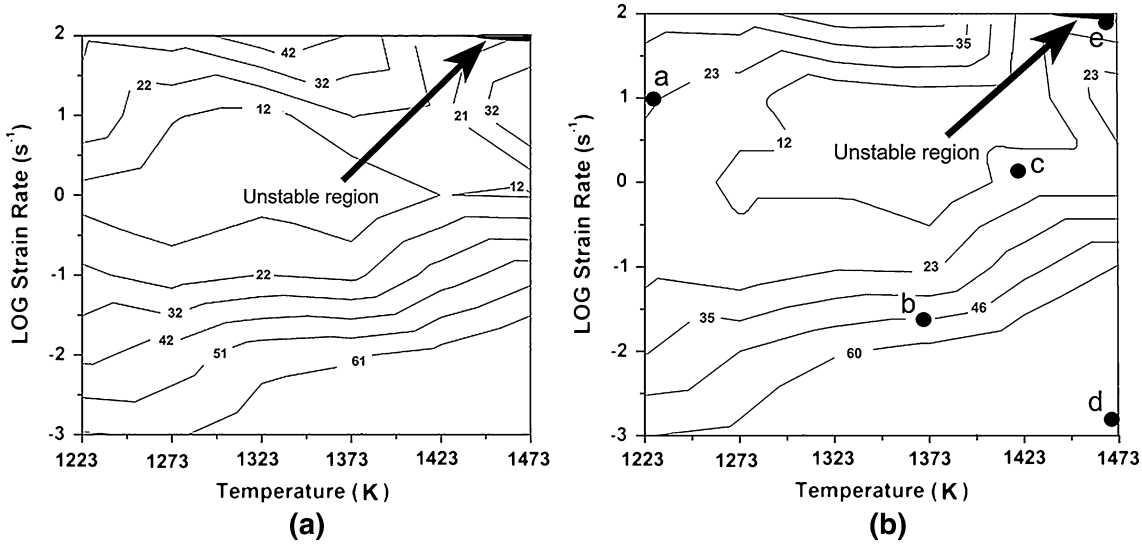

Fig. 9—Sin h-based processing map of the material drawn by the superposition of power dissipation map and instability map at the typical strains of (*a*) 0.3 and (*b*) 0.7.

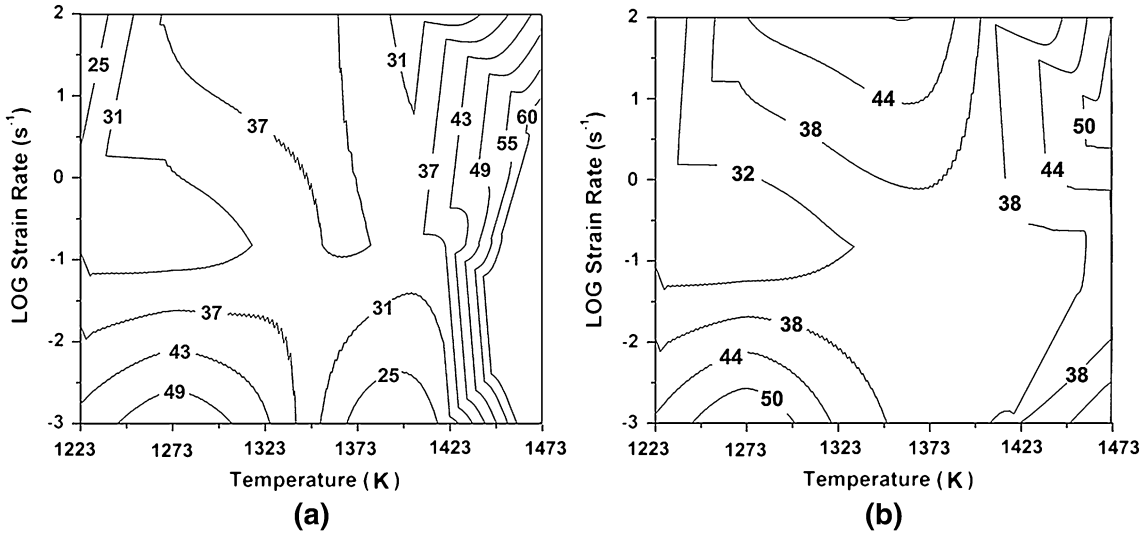

Fig. 10—Conventional processing maps developed based on Eqs. [12] and [15] at strains of (*a*) 0.3 and (*b*) 0.7.

is interesting to note that with increasing strain rate shown in Figure 9, as DRV in ferrite becomes weaker, the value of η decreases down to a minimum of 12 pct at the strain rate about 1 s^{-1}. As strain rate increases over 1 s^{-1}, load is more transmitted to austenite, which causes it to work harden and then soften. This scenario fits better with the PDM in the sin h-based processing maps than in the conventional ones. Another point that should be highlighted is that the instability region at 1200 °C (1473 K) and 100 s^{-1} is more consistent with the low η value of 12 pct in Figure 9. The same regime in the conventional processing maps of Figure 10 is located where the average value of η is as high as 50 pct. As a result, it seems that the processing map constructed on the hyperbolic sine function fits better with the mechanical behavior of the material. However, microstructural observations are needed to be used to validate the mechanical predictions.

C. *Validation of the Processing Map Using Microstructural Observations*

Figure 11 exhibits micrographs obtained from the different regions of the processing map alphabetically named as a, b, c, d, and e. Figure 11(a) indicates that at 1223 K (950 °C)—10 s^{-1}, there is no mark of instability, and the visible boundaries in the ferritic matrix imply the occurrence of DRV while. in small austenite islands, DRX is likely prohibited. Fan *et al.*[25] and Momeni *et al.*[26] stated that in duplex stainless steels, ferrite precedes austenite in the accommodation of strain and thereby softening. Therefore, the deformation and

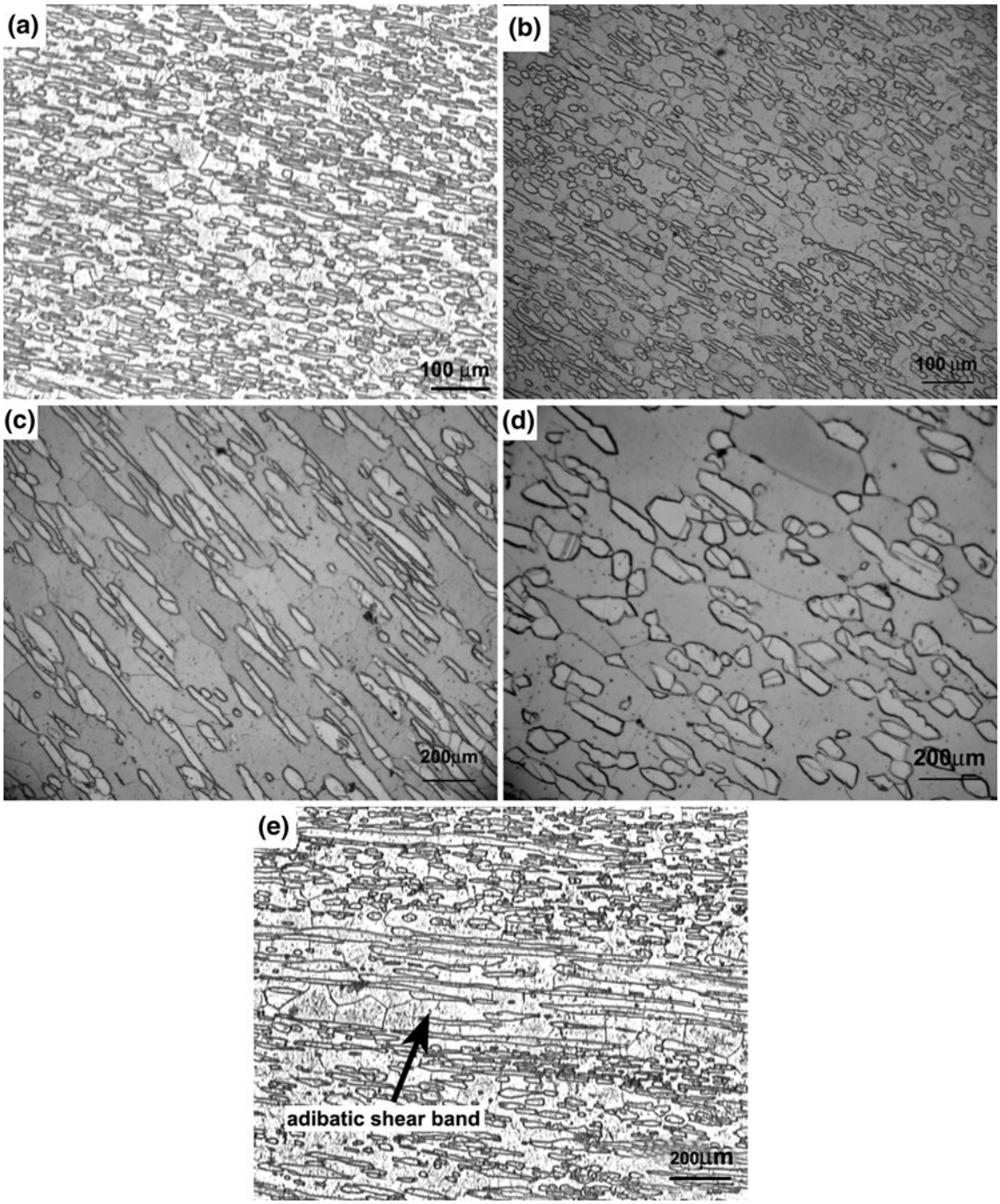

Fig. 11—Optical micrographs of samples hot deformed at (*a*) 1223 K (950 °C), 10 s^{-1}, (*b*) 1373 K (1100 °C), 0.01 s^{-1}, (*c*) 1423 K (1150 °C), 0.1 s^{-1}, (*d*) 1473 K (1200 °C), 0.001 s^{-1} and (*e*) 1473 K (1200 °C), 100 s^{-1}. "a," "b," "c," "d," and "e" correspond to the same letters shown in Fig. 9(b).

restoration processes in ferrite may delay or inhibit them in the coexistent austenite phase. However, the pancaked austenite islands reflect that this phase has also undergone a part of imposed plastic strain. By increasing temperature and decreasing strain rate, respectively, to 1373 K (1100°C) and 0.01 s^{-1}—denoted by "b"—the value of η increases to about 46 pct. It is because at high temperatures and low strain rates, both austenite and ferrite are able to be softened by the corresponding mechanisms. This is also evident in Figure 11(b) where more sharpened boundaries in the matrix as well as in the austenite islands are attributed to DRV and DRX, respectively. Figure 11(c) indicates that in the region "c" that corresponds to 1423 K (1150 °C) and 0.1 s^{-1}, austenite is more elongated in the deformation direction suggesting less softening capacity and therefore lower value of η. When temperature is increased again to 1473 K (1200 °C) and strain rate decreases to 0.001 s^{-1},

the region indexed as "d" is characterized by a η value as high as 60 pct. The corresponding microstructure in Figure 11(d) exhibits mostly the globular austenite island instead of the string-form at high strain rates and sharp boundaries in both ferrite and austenite, reflecting expeditious contributions of DRV and DRX toward a kind of superplastic deformation. As a comparison, in Figure 10(b), the same region denoted by "d" [1473 K (1200 °C)—0.001 s^{-1}] corresponds to about 38 pct energy consumption through microstructural changes. It is therefore concluded that the extensive microstructural changes that were observed in Figure 11(d) are more consistent with the value of 60 pct for η in the sin h-based processing map than with the value of 38 pct in Figure 10(b).

At the same temperature of 1473 K (1200 °C) and very high strain rate of 100 s^{-1} indicated by "e" in the sin h-based processing map (Figure 9(b)), the only region of flow instability is predicted by the mechanical testing. Figure 11(e) shows microstructure obtained from the instability region denoted by "e." As observed, although there is no indication of cracking or void formation in the matrix or the in the austenite islands, but the austenite phase has been locally elongated that introduces the formation of an adiabatic shear band. Meanwhile, the ferrite grains in the adiabatic shear band are considerably larger and are separated by very sharp boundaries. Momeni *et al.*[26] observed that ferrite can bear a kind of continuous dynamic recrystallization (CDRX) when DRV extends to high strains. This process becomes possible by the micromechanism of subgrains growth and coalescence. At high temperatures and high strain rates the conduction rate of deformation heating to the adjacent tools cannot keep pace with the deformation rate. Therefore, it gives rise to the entrapment of extra heat into the sample and the local decline of flow stress. The adiabatic shear band is a region where the local decline of flow stress due to adiabatic heating causes the strain to be localized. As ferrite is softer than austenite at hot working temperatures, in this region, the extra strain is preferably accommodated by ferrite and results in extended DRV and CDRX. In general, due to the localization of strain the adiabatic shear band is known as a variant of instability during hot working. In Figure 9(b), this region is accompanied by a the lowest value of η as 12 pct; while in Figure 10(b), not only has the region not been marked as instable, but also a high average value of η ranging from 40 to 50 pct is observed. Consequently, the metallographic observations are more consistent with the results of the sin h-based processing maps.

IV. CONCLUSIONS

The processing maps of 2205 duplex stainless steel were developed based on the hyperbolic sine and power-law constitutive equations. The most important results are listed below:

1. The flow stress of the studied material was connected to strain rate and temperature by the hyperbolic sine function at both low and high strain levels.
2. The PDM, instability map, and processing map were developed for the strains of 0.3 and 0.7 based on the hyperbolic sine constitutive equation as well as by the conventional method.
3. The efficiency of power dissipation (η) varied from 12 to 60 pct over the studied temperatures and strain rates. The highest value of η was obtained at strain rates below 0.01 s^{-1}, whereas the lowest value of η was observed at the intermediate strain rates.
4. The only instability region on the sin h-based processing map was observed in the range from 1423 K to 1473 K (1150 °C to 1200 °C) and at the strain rate of 100 s^{-1}. This was found to be due to the development of adiabatic shear bands. The conventional processing map did not predict any instability region.
5. The power dissipation and instability maps developed by the hyperbolic sine function were more consistent with the microstructural observations than the corresponding maps developed by the conventional method.

REFERENCES

1. G.R. Ebrahimi, H. Keshmiri, A. Momeni, and M. Mazinani: *Mater. Sci. Eng. A*, 2011, vol. A528, pp. 7488–93.
2. A. Dehghan-Manshadi, M.R. Barnett, and P.D. Hodgson: *Metall. Mater. Trans. A*, 2008, vol. 39A, pp. 1359–70.
3. M. Yazdani, S.M. Abbasi, A. Momeni, and A. Karimi Taheri: *Mater. Des.*, 2011, vol. 32, pp. 2956–62.
4. R. Raj: *Metall. Trans. A*, 1981, vol. 12A, pp. 1089–97.
5. B. Bozzini and E. Cerri: *J. Nucl. Mater.*, 2002, vol. 328, pp. 344–47.
6. Y.V.R.K. Prasad, H.J. Gegel, S.M. Doraivelu, J.C. Malas, J.T. Morgan, L.A. Lark, and D.R. Barker: *Metall. Trans. A*, 1984, vol. 15A, pp. 1883–92.
7. H. Ziegler:, in *Progress in Solid Mechanics*, I.N. Sneedon and R. Hill, eds., Wiley, New York, NY, 1963, vol. 4, pp. 63–193.
8. Y.V.R.K. Prasad: *Ind. J. Technol.*, 1990, vol. 28, pp. 435–51.
9. Y.V.R.K. Prasad and T. Seshacharyulu: *Int. Mater. Rev.*, 1998, vol. 43, pp. 243–58.
10. Y.V.R.K. Prasad: *J. Mater. Eng. Perform.*, 2003, vol. 12, pp. 638–45.
11. I. Philipart and H.J. Rack: *Mater. Sci. Eng.*, 1998, vol. A254, pp. 253–67.
12. A. Momeni, S.M. Abbasi, and H. Badri: *Appl. Math. Model.*, 2012, vol. 36, pp. 5624–32.
13. Y.C. Lin, M.S. Chen, and J. Zhong: *Comp. Mater. Sci.*, 2008, vol. 42, pp. 470–77.
14. Y.C. Lin and X.M. Chen: *Mater. Des.*, 2011, vol. 32, pp. 1733–59.
15. A. Momeni, K. Dehghani, G.R. Ebrahimi, and H. Keshmiri: *Metall. Mater. Trans. A*, 2010, vol. 41A, pp. 2898–904.
16. M. Mirzaee, H. Keshmiri, G.R. Ebrahimi, and A. Momeni: *Mater. Sci. Eng.*, 2012, vol. 551, pp. 25–31.
17. F. Garofalo: *Fundamentals of Creep and Creep-Rupture in Metals*, Macmillan Company, New York, NY, 1966.
18. A. Momeni and K. Dehghani: *Metall. Mater. Trans. A*, 2011, vol. 42A, pp. 1925–32.
19. S.V.S. Narayana Murty, B. Nageswara Rao, and B.P. Kashyap: *Model. Simul. Mater. Sci. Eng.*, 2002, vol. 10, pp. 503–20.
20. S.V.S. Narayana Murty and B. Nageswara Rao: *Mater. Sci. Eng.*, 1998, vol. A254, pp. 76–82.
21. S.V.S. Narayana Murty and B. Nageswara Rao: *Mater. Sci. Technol.*, 1998, vol. 14, pp. 835–37.
22. S.V.S. Narayana Murty, M.S. Sarma, and B. Nageswara Rao: *Metall. Mater. Trans. A*, 1997, vol. 28A, pp. 1581–82.
23. A. Momeni and K. Dehghani: *Mater. Sci. Eng.*, 2011, vol. 528, pp. 1448–54.
24. R. Ebrahimi and A. Najafizadeh: *Int. J. ISSI*, 2004, vol. 1, pp. 1–7.
25. G.W. Fan, J. Liu, P.D. Han, and G.J. Qiao: *Mater. Sci. Eng.*, 2009, vol. A515, pp. 108–12.
26. A. Momeni, K. Dehghani, and X.X. Zhang: *J. Mater. Sci.*, 2011, vol. 47, pp. 2966–74.